Supporting Information

High CO_2/N_2 and CO_2/CH_4 selectivity in a chiral metal-organic framework with contracted pores and multiple functionalities

Xiaoxia Lv,[‡] Liangjun Li,*[,§] Sifu Tang,[‡] Chao Wang,[‡] Xuebo Zhao*[,‡]

Received (in XXX, XXX) Xth 20XX, Accepted Xth XXX 20XX
DOI: 10.1039/b000000x

[§]Institute of Unconventional Hydrocarbon and New Energy Sources, China University of Petroleum (East China), Qingdao 266580, China
E-mail: liliangjun1982@hotmail.com
[‡]Qingdao Institute of Bioenergy and Bioprocess Technology, Chinese Academy of Sciences, Qingdao 266101, China
Fax: +86 0532-80662728; E-mail: zhaoxb@qibebt.ac.cn

Contents:

S1. Experimental section

1. Materials and Instrumentation

All the chemicals were obtained from commercial sources and used without further purification. Elemental analyses for C, H, and N were performed on a German Elementary Vario EL cube instrument. Infrared spectra (IR) were recorded on a Nicolet 6700 FTIR spectrometer in the region 4000−400 cm^{-1} using KBr pellets. Thermogravimetric analyses (TGA) were carried out on a NETZSCH STA 449F3 unit at a heating rate of 20 °C min^{-1} under nitrogen atmosphere. Solution ^1H NMR spectra were recorded on a Bruker AVANCE-III NMR (600 MHz). Power X-ray diffraction (PXRD) patterns were collected by a D8 Advance X-ray diffractometer using Cu-Kα radiation (λ = 0.154 nm) radiation at room temperature. Sorption isotherms were measured over pressure range from vacuum to 20 bar by a gravimetric adsorption apparatus (Intelligent Gravimetric analyzer, IGA-001). The mixed gas adsorption experiments were conducted on IGA-001, using the same experimental procedure and experimental conditions as single-component gas sorption experiments, except that binary- component gas mixtures were used. The composition of the feed gas was analyzed on a gas chromatograph (Agilent Technologies).

2. Syntheses

Synthesis of 4,4'-(5,6-dimethyl-1H-benzo[d]imidazole-4,7-diyl)dibenzoic acid (H_3L)

4-(ethoxycarbonyl)phenylboronic acid was prepared according to the procedure described in the literature[1]. 4,7- dibromo-5,6- dimethyl- 1H- benzo[d] imidazole was prepared according to the procedure described in the literature[2]. The ligand 4,4'-(5,6- dimethyl-1H- benzo [d]imidazole- 4,7- diyl)dibenzoic acid (H_3L) was synthesized by Suzuki-coupling reaction of 4,7- dibromo -5,6- dimethyl- 1H- benzo [d]imidazole and 4- (ethoxycarbonyl) phenylboronic acid. 4,7- dibromo- 5,6- dimethyl- 1H-benzo [d]imidazole (3.04 g, 10 mmol), 4-(ethoxycarbonyl)phenylboronic acid (4.658 g , 24mmol) and K_3PO_4 (21.0 g, 100

mmol) were mixed in a 500 ml three-neck flask. Then the mixture was degassed at Schlenk line and recharged with Nitrogen. The evacuate-charge procedure was repeated for at least three times to ensure the inert gas atmosphere of the reaction system. After introducing $Pd(PPh_3)_4$ (500 mg, 0.43 mmol), and dioxane (300 ml), the mixture of reactants and catalyst was heated to 100 °C and stirred for 72 hours under the nitrogen atmosphere. After cooling to room temperature removed the solvent and extracted with $CHCl_3$ (50 ml) for three times. Then, the extraction was washed with water, dried with anhydrous Na_2SO_4 and evacuated under vacuum. The resulting yellow oil was purified by silica gel column using elute of petroleum / ethyl acetate (3/1, v/v,). The obtained white solid was hydrolyzed with the NaOH (12 g, 300 mmol) in the solution of THF/EtOH/H_2O (2/2/3, 300 ml). After acidified with concentrated HCl (adjust the pH value of the solution to about 4), a white precipitate was separated by filtration and dried at 60 °C in vacuum. ^{1}HNMR (d^6-DMSO, 600MHz): δ = 13.0 (s, 2H, -*COOH*), 12.3 (m, 1H, -*NH*-), 8.08 (d, 4H, *Ar-H*), 8.04 (s, 1H, -*CH*-), 7.54 (d,4H, *Ar-H*), 2.20 (s, 6H, -CH_3). Selected IR data (cm-1): ν= 3442 (s), 3152 (w), 2926 (w), 2852 (w), 1682 (vs), 1632 (w), 1608 (m), 1562 (w), 1497 (w), 1385 (s), 1278 (m), 1176 (m), 1099 (w), 1080 (s), 1034 (w), 1014 (m), 986 (w), 928 (w), 879 (w), 850 (m), 793 (m), 770 (s), 706 (m), 629 (w), 608 (w), 530 (m).

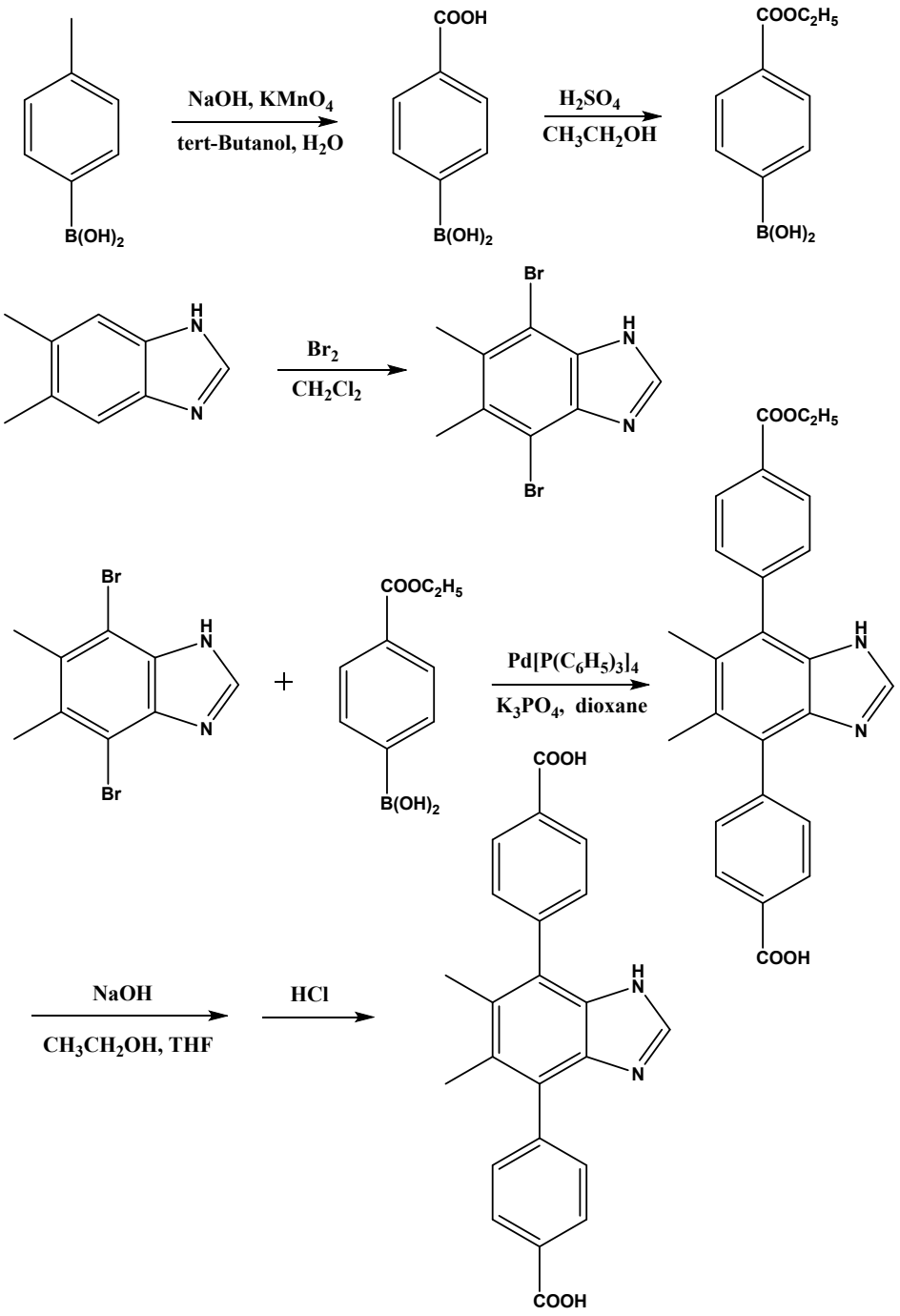

Scheme S1 The synthesis of H_3L

Synthesis of [Zn(HL)·H_2O]·DMA (1)

A mixture of H_3L (0.03864 g, 0.1 mmol) and $ZnNO_3·6H_2O$ (0.1017 g, 0.36 mmol) were dissolved in DMA/H_2O (1/1) (12 mL) and stirred at room temperature for 30 minutes in a Teflon-lined autoclave (23 mL). Then the autoclave was heated at 100 °C for 2 days. After cooled to room temperature slowly (12 h), colorless crystals of compound 1 were filtered off and were washed with DMA. The yield is about 74 %

based on H_3L. Elemental analysis for $ZnC_{27}H_{27}N_3O_6$, calcd (%): C58.44, H 4.90, N 7.57. Found (%): C 58.60, H 4.93, N 7.56. Selected IR data (cm-1): ν = 3442 (s), 2926 (w), 2848 (w), 1610 (vs), 1543 (m), 1504 (w), 1389 (vs), 1327 (w), 1254 (m), 1177 (m), 1101 (w), 1016 (m), 975 (w), 860 (w), 778 (s), 715 (m), 630 (w), 610 (w), 528 (m).

3. Single crystal X-ray diffraction

Crystal data for compound **1** was collected on a Bruker SMART APEX Ⅱ CCD diffractometer with graphite monochromatic Mo-Kα radiation (λ=0.71073Å) at room temperature. Data acquisition and integration were undertaken with the SMART and SAINT programs respectively. Multi-scan empirical absorption corrections were applied to the data using the SADABS program [3]. The structure was solved by direct method using SHELXS [4] and refined by full-matrix least-squares fitting on F^2 by SHELXL-97 [5]. Anisotropic thermal parameters were used for all the non-hydrogen. Organic hydrogen atoms were added theoretically, while hydrogen atoms of water were added by Fourier syntheses and in a fixed geometrically. All the hydrogen atoms were refined isotropically. The guest molecules were disordered and difficult to locate and refine. Therefore, we removed those disordered guest molecules with the SQUEEZE procedure [6]. Crystallographic details for compound **1** were summarized in table S1. Selected bond lengths and bond angles were displayed in Table S2. Data for the crystal structure has been deposited at the Cambridge Crystallographic Data Centre (CCDC 963443), these data are obtained free of charge via Internet at www.ccdc.cam.ac.uk.

S2. Single crystal X-ray crystallography

Table S1 Crystallographic data for **1**

Compound	1(squeeze)
Formula	$C_{23}H_{18}N_2O_5Zn$
Formula weight	467.76
Cryst system	Orthorhombic
Space group	*P2(1)2(1)2(1)*
***a* (Å)**	6.215(2)
***b* (Å)**	20.656(8)
***c* (Å)**	25.022(10)
***α* (deg)**	90.00
***β* (deg)**	90.00
***γ* (deg)**	90.00
Z	4
***V* (Å^3)**	3213(2)
Density (gm/cm^3)	0.967
Absorption coefficient (mm^{-1})	0.789
F(000)	960
Reflections collected/unique	13374 / 5551 / 0.0921
Data/restraints/parameters	5551 / 30 / 245
Final R indices [R1>2σ(*I*)]	*R1*=0.0794, *wR2*=0.1804
GOF on F^2	1.081
Largest diff. peak and hole(e/Å^3)	0.801 and -0.671

Table S2 Selected Bond Lengths (Å) and Angles (deg) for **1**

compound **1**[a]					
Zn1-N1C	1.979(7)	Zn1-O1	1.987(5)	Zn1-O4D	2.000(6)
Zn1-O1W	2.058(5)	N1-Zn1B	1.979(7)	O4-Zn1A	2.000(6)
N1C-Zn(1)-O1	132.7(3)	N1C-Zn1-O4D	100.4(3)	O1-Zn1-O4D	107.3(3)
N1C-Zn1-O1W	107.6(3)	O1-Zn1-O1W	107.0(2)	O4D-Zn1-O1W	95.6(2)

Equivalent position codes: A) x-1/2, -y+3/2, -z+2; B) x-1/2, -y+3/2, -z+2; C) -x+3/2, -y+1, z-1/2; D) x+1/2, -y+3/2, -z+2

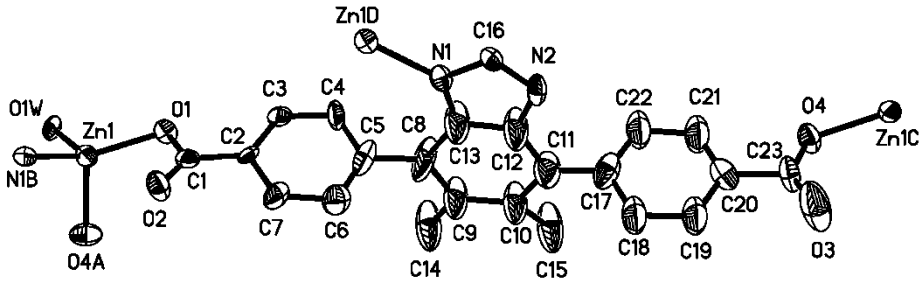

Fig. S1 The coordination environments of the Zn(II) ions and the ligand in **1**. symmetry codes: A）: -x+3/2, -y+1, z+1/2；B）: x-1/2, -y+3/2, -z+2；C）: -x+3/2, -y+1, z-1/2；D）: x+1/2, -y+3/2, -z+2)

As shown in Fig. S2, the asymmetric unit contains one zinc ion, one part deprotonated L^{2-}, one coordinated aqua ligand and some discrete solvent molecules. Zinc ion is surrounded by three oxygen atoms and one nitrogen atoms to form a slightly distorted tetrahedral geometry. The coordinated oxygen atoms come from two carboxylic groups with the monodentate coordination mode and one terminal water molecule and one nitrogen atom from the imidazole group. The length of Zn-N bond is 1.979, while Zn-O bands is within the range of 1.987- 2.058.

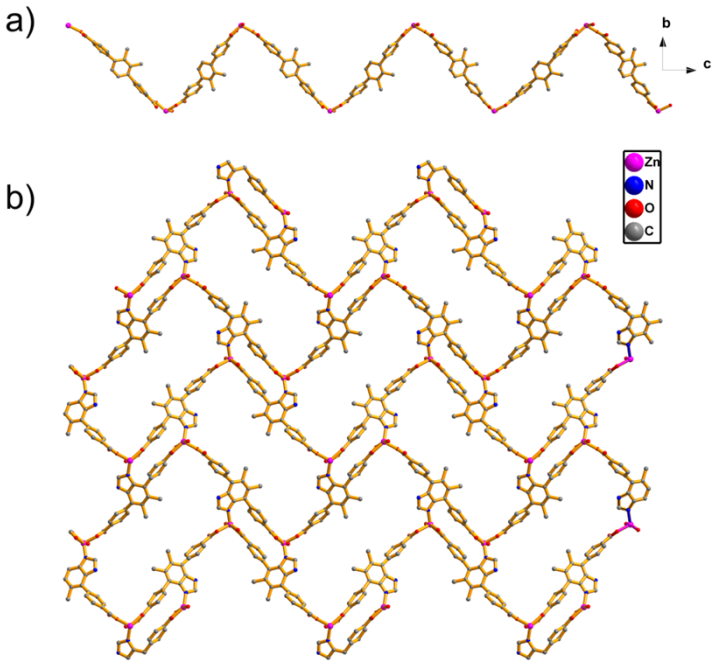

Fig.S2 (a) The 1D chain assemblied by dicarboxylate part of ligand and metal ions ; (b) The ball and stick presentation of **1** viewing from *a* axis.

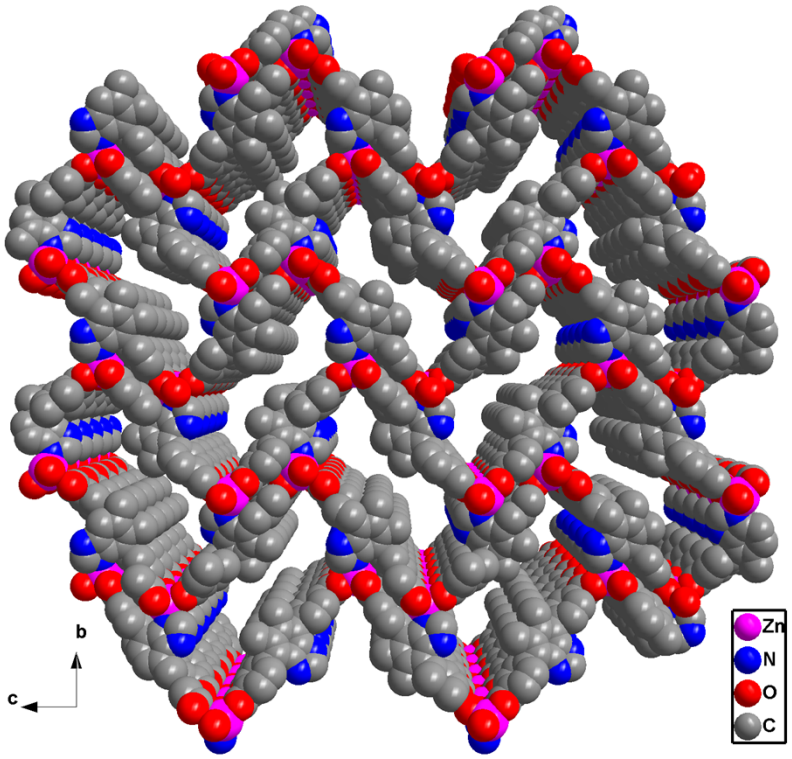

Fig.S3 The perspective view of pores of compound **1** viewing from *a* axis

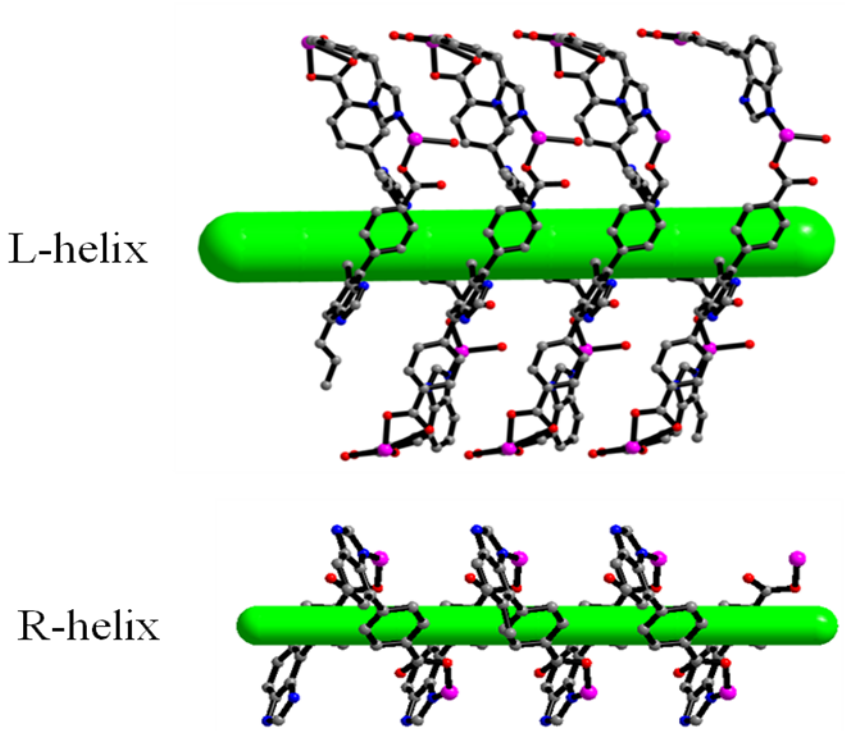

Fig. S4 The L-helix and R-helix of compound **1**

S3. IR, TGA and PXRD patterns

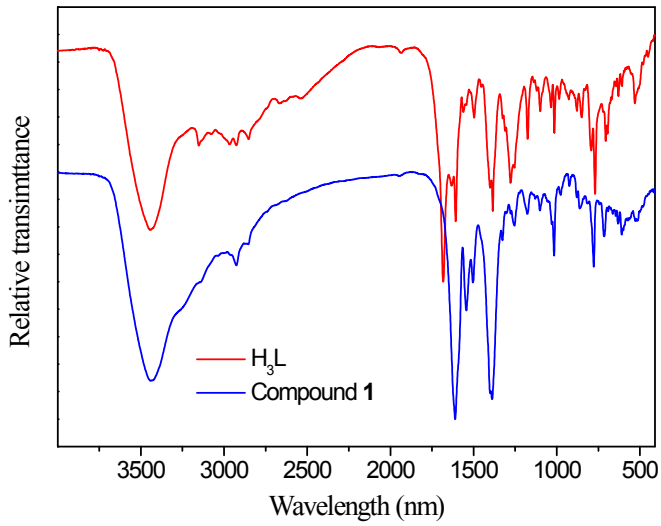

Fig.S5 IR sprctra of compound **1**

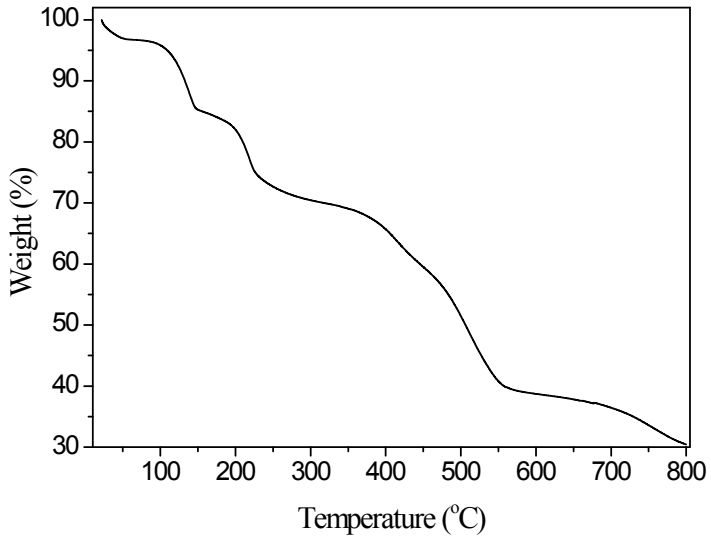

Fig. S6 TGA curve of compound **1** under N_2 atmosphere from room temperature to 800 ℃

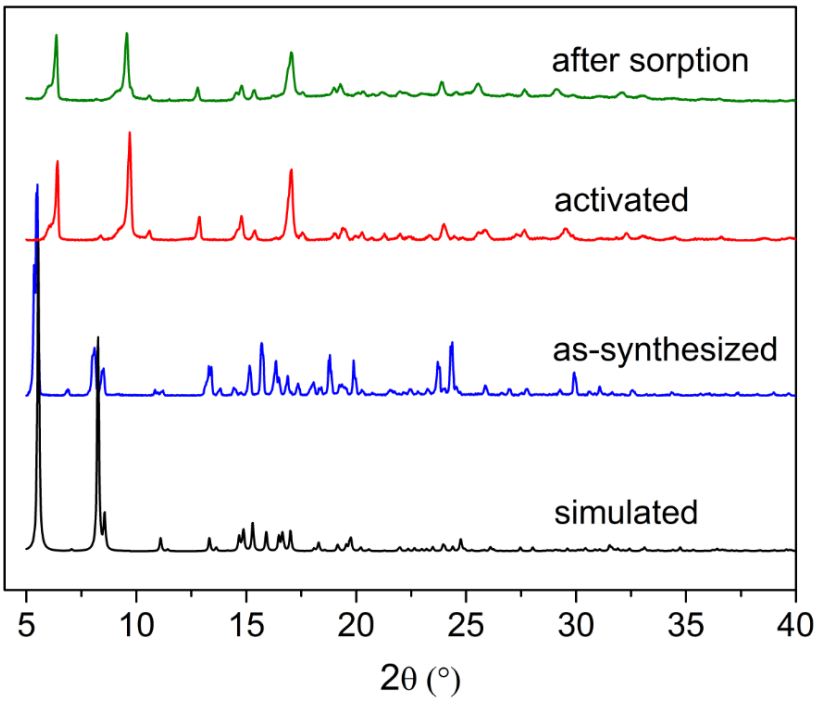

Fig. S7 Simulated PXRD pattern from crystallographic data (black) and PXRD patterns of the as-synthesized sample (blue), the activated sample (red) and the sample after sorption (green)

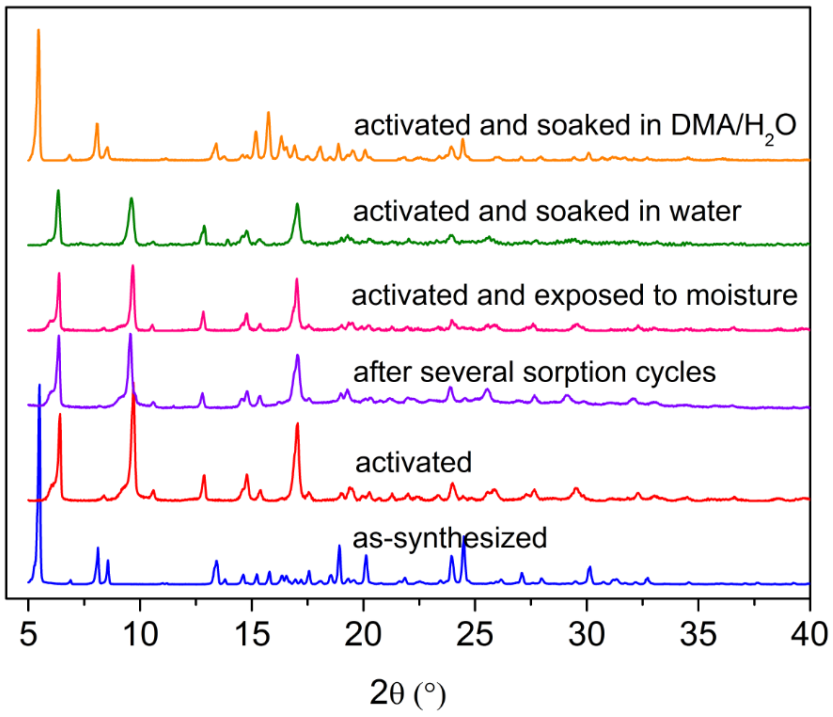

Fig. S8 PXRD patterns of the sample after several sorption cycles (violet), activated and exposed to moisture for 24 hours (magenta), activated and soaked in water for 24 hours (green), activated and immersed in DMA/H_2O (1/1, v/v) solutions for 24 hours (orange).

S4. Gas isotherms and characterization of pore structure

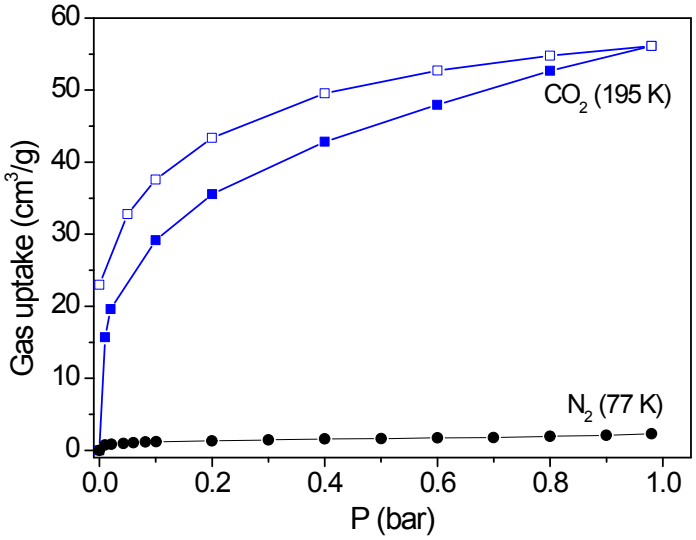

Fig. S9 CO_2 and N_2 isotherms at low temperatures

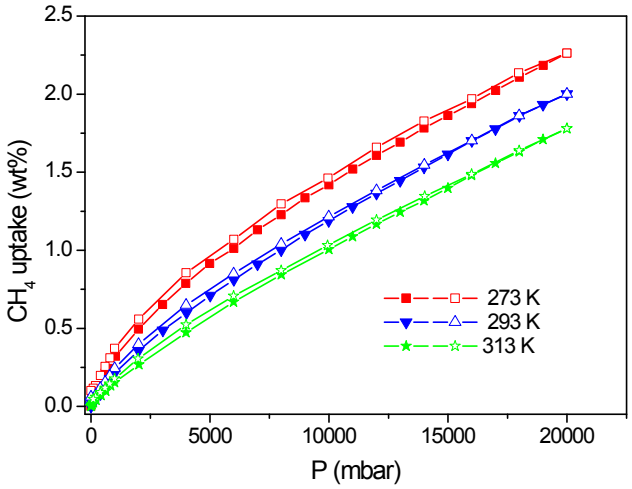

Fig. S10 CH_4 isotherms of 1a at 273 K, 293 K and 313 K

Calculation of BET surface area

The BET surface area of **1a** was calculated by using Brunauer-Emmett-Teller equation from CO_2 adsorption isotherm at 273 K (as shown in equation 1).

$$\frac{P}{V(P_0 - P)} = \frac{1}{CV_m} + \frac{C-1}{CV_m} \cdot \frac{P}{P_0} \qquad (1)$$

Using the CO_2 isotherm of **1a** at 273 K, the term $P/V(P_0-P)$ was plotted and linear fitted with P/P_0 in the pressure range of $0.05 < P/P_0 < 0.26$, as shown in Fig. S8.

According to the Brunauer-Emmett-Teller equation, the term $(C-1)/ CV_m$ and $1/CV_m$ are equal

to the slope and the intercept of the fitted line, respectively.

$$\frac{C-1}{CV_m} = 0.69093 \qquad \frac{1}{CV_m} = 0.01362$$

So, we can obtain the value of C and V_m for **1a** as following:

$$C = 51.7291 \qquad V_m = 1.4193 \text{ mmol g}^{-1}$$

The BET surface area is calculated by the equation 4.

$$S_{BET} = V_m \cdot A \cdot \sigma_m \tag{2}$$

Where A is the Avogadro constant (6.023×10^{23} mol^{-1}), σ_m is sectional area of one CO_2 molecular (2.16×10^{-19} m^2). So the BET surface area of **1a** is 185 m^2 /g.

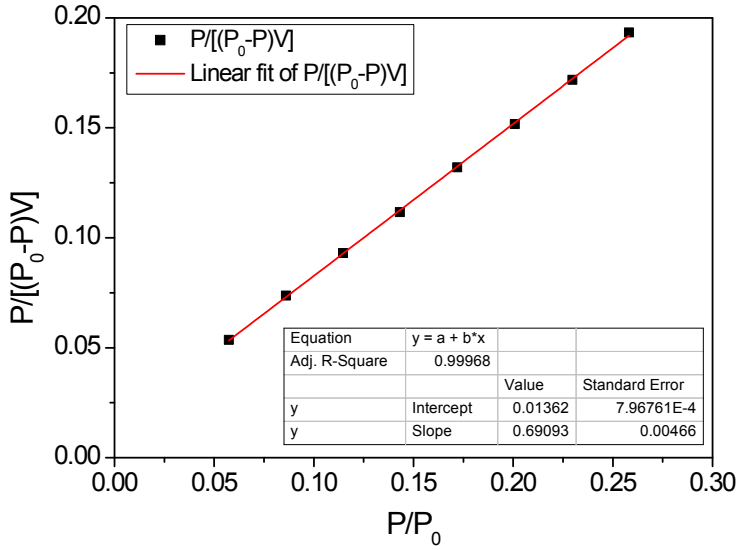

Fig. S8 BET plot of **1a** for CO_2 adsorption at 273 K in the linear region ($0.05<P/P_0<0.26$)

Calculation of Pore volume

Given the fact that **1a** takes up no significant N_2 at 77 K due to diffusion difficulty of N_2 molecules in ultra narrow pores under cryogenic conditions, the pore volume of compound **1a** cannot be obtained by conventional method using N_2 as adsorptive. However, the pore volume of **1a** can be determined from the Dubinin-Radushkevich (DR) equation using CO_2 as adsorptive,[7] which is proposed as an effective method to analysis pore texture of microporous materials, especially the materials with ultra narrow pores that N_2 has kinetic restrictions.[8] Therefore, in this paper, the DR equation (equation 3) is employed to depict the characteristic curve for **1a**.

$$V = V_0 \times \exp\left[-\left(\frac{\varepsilon_{ref}}{E_0}\right)^2\right], \text{ with } \varepsilon_{ref} = \frac{RT\ln(P_s/P)}{\beta} \tag{3}$$

Where V ($cm^3 \cdot g^{-1}$) is the volume adsorbed at a pressure P (bar), V_0 ($cm^3 \cdot g^{-1}$) is the

micropore volume, ε_{ref} (kJ·mol^{-1}) is the adsorption potential for a reference adsorbate, E_0 (kJ·mol^{-1}) is the characteristic energy, β is the affinity parameter (In the case of CO_2 adsorption at 273 K, the value of β is proposed to be 0.35[7]).

According to DR equation, the characteristic curve for adsorption of CO_2 on **1a** can be obtained. As shown in Fig. S9, the characteristic curve of **1a** composed of two parts with different trends. The curve with high adsorption potential in the lower pressure range is linear, while the curve with low adsorption potential in the higher pressure range is non-linear. Considering the fact that **1a** takes up no significant amount of N_2 at 77 K, so there is no meso- or macro- pores involved in **1a**. Therefore, the linear part on characteristic curve in low pressure range (P< 1 bar) could be induced by the ultra micropores at low CO_2 loadings, while the non-linear curves in higher pressure range (P> 1 bar) could be attributed to the pore expansion when accommodating larger amount of CO_2.

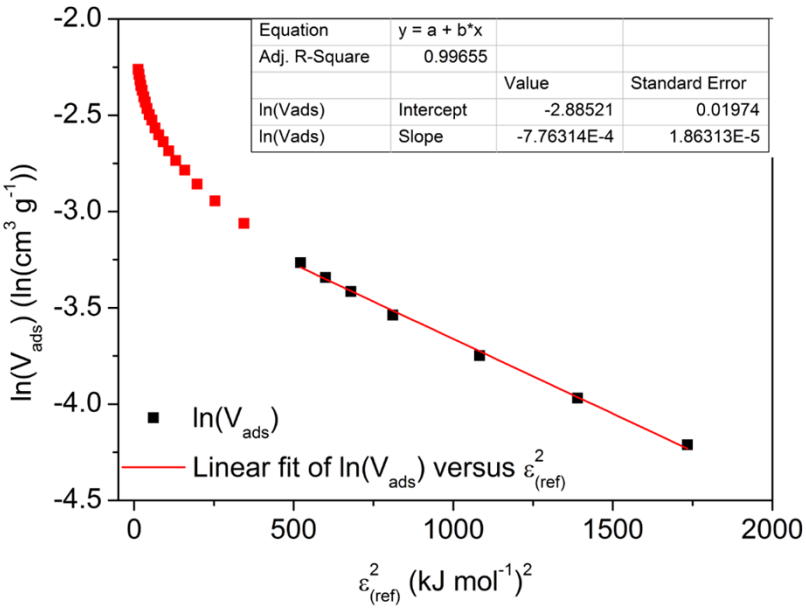

Fig. S9 Characteristic curve for adsorption of CO_2 at 273 K on **1a**

So, the ultra micro pore structure of compound **1a** (V_0) can be characteristic using the linear part of the characteristic curve. The micropore volume is 0.0558 cm^3 g^{-1}, which is a very small pore volume compared to the pore volume of the as-synthesized MOF (the pore volume calculated from crystallographic data is 0.467 cm^3·g^{-1}). The characteristic energy E_0 can be calculated as 35.89 kJ·mol^{-1}. Based on the fact that the activated MOF is a crystalline material and only one type of pore is involved in this MOF, the pore structure can be deemed as homogeneous. Therefore, the pore width of **1a** can be determined from Stoeckli equation[9] (equation 4).

$$L = \frac{10.8}{E_0 - 11.4} \qquad (4)$$

With the characteristic energy between 20 and 42 kJ·mol^{-1}, where L (nm) is the

mean pore width, E_0 (kJ·mol^{-1}) is the characteristic energy.

So, the pore width of **1a** can be calculated as 0.42 nm which is an ultra narrow pore width that is agreeable with the sorption behaviors. The substantial reduce of the pore volume and pore width of the activated MOF compared to the as-synthesized MOF clearly states that the pore of the pore of this MOF has been contracted upon activation.

S5. Calculation procedures of selectivity from IAST

The separation selectivity of gas mixtures are calculated from the single-component gas isotherms by using the ideal adsorbed solution theory (IAST).[10] Firstly, CO_2 and CH_4 adsorption Isotherms are fitted by dual site Langmuir-Freundlich model (DSLF), using the following equation:

$$N = N_1 \times \frac{b_1 P^{1/n_1}}{1 + b_1 P^{1/n_1}} + N_2 \times \frac{b_2 P^{1/n_2}}{1 + b_2 P^{1/n2}} \quad (5)$$

where P is the pressure of bulk gas at equilibrium with adsorbed phase, N_1 and N_2 are maximum loading in sites 1 and 2, b_1 and b_2 are the affinity constants of sites 1 and 2, and n_1 and n_2 are used to characterize the deviation from the simple Langmuir equation.

The fitting parameters of DSLF equation as well as the correlation coefficients (R^2) are listed in Table S3. The experimental and fitted isotherms for CO_2, CH_4 and N_2 at 273 K are depicted in Fig. 3a.

Table S3. Equation parameters for the DSLF isotherm model for CO_2 and CH_4 Adsorption Isotherms at 273 K

Adsorbates	N_1	b_1	$1/n_1$	N_2	b_2	$1/n_2$	R^2
CO_2	6.07797	0.17811	0.35917	8.06154	0.0001227	2.05419	0.99997
CH_4	0.46492	0.40654	0.95495	4.42869	0.00886	1.07131	0.99984
N_2	0.7612	0.06527	0.63631	4.05585	0.006	1.00609	0.99996

IAST is a method for predicting the adsorption equilibria for components in a mixture derived by Myers and Prausnitz[11] using single-component adsorption data. Which is based upon three assumptions: (i) that the same surface area is available to all adsorbates, (ii) that the adsorbent is inert, and (iii) that the multicomponent mixture behaves as an ideal solution (such that the mean strength of interaction is equal between all molecules of the solution) at constant spreading pressure and temperature.

From the IAST, the spreading pressure π is given by：

$$\pi_i^{\,0}(p_i^{\,0}) = \frac{RT}{A}\int_0^{P_i^0} q \cdot d\ln P \quad (6)$$

$$\pi^* = \frac{\pi A}{RT} = \int_0^{P_i^0} \frac{q_i}{P} dP \tag{7}$$

Where A is the specific surface area of the adsorbent, π and π^* are the spreading pressure and the reduced spreading pressure, separately. is the gas pressure of component *i* that corresponding to the spreading pressure π of the gas mixture.

At a constant temperature, each component has the same spreading pressure:

$$\pi = \pi_i = \pi_j (i \neq j) \tag{8}$$

From Raoult's law for ideal solutions, the relation between the mole fraction in the gaseous phase y_i, and the mole fraction in the adsorbed phase x_i :

$$P \times y_i = P_i^0(\pi^*) \cdot x_i \tag{9}$$

Where is the pressure of the single component in its standard state which is fixed by the spreading pressure of the mixture according to Equation (8). The total amount adsorbed of the mixture, q_t, is determined using the expression

$$\frac{1}{q_t} = \sum_i^n \frac{x_i}{q_i^0(P_i^0)} \tag{10}$$

Where $q_i^0(P_i^0)$ are the adsorbed amounts of the single-component isotherms.

The selectivity for component *j* relative to component *i* is defined as:

$$S_{ij} = \frac{P_i^0}{P_j^0} = \frac{Py_i / x_i}{Py_j / x_j} = (\frac{x_j}{y_j})(\frac{y_i}{x_i}) \tag{11}$$

Where x_j and x_i are, respectively, the mole fractions of components *j* and *i* in the adsorbed phase and y_j and y_i are the mole fraction of components *j* and *i* in the bulk phase, respectively.

S6. Calculation procedures of isosteric adsorption enthalpy

1. Isosteric heats of adsorption (Q_{st}) at zero surface coverage

The Virial equation can be written in the following form:

$$\ln(n / P) = A_0 + A_1 \cdot n + A_2 \cdot n^2 + A_3 \cdot n^3 + \cdots \tag{12}$$

Where *n* is the amount adsorbed at pressure *p* and the first Virial coefficient, A_0 is a constant related to the Henry's law constant. In the low pressure range, the higher terms (A_2, A_3… etc) in the Virial equation could be ignored at low surface coverage. As shown in the plots, the term ln(n/P) shows the nearly linear relationship with adsorption amounts (as shown in Fig. S9-11 for CO_2 and in Fig. S13-15 for CH_4). Therefore, the values of the first Virial coefficient (A_0) and the second Virial

coefficient (A_1) which reflect the adsorbate-adsorbent interaction and adsorbate-adsorbate interactions, respectively, can be obtained from the linear fit of ln(n/P) versus n.

The isosteric heats of adsorption at zero surface coverage ($Q_{st\ (n=0)}$) can be obtained from the gradient of the graph of the first Virial coefficient (A_0) versus 1/T (Fig. S12 for CO_2 and Fig. S16 for CH_4). The $Q_{st\ (n=0)}$ for CO_2 and CH_4 can be calculated as 43.7±3.1 and 16.4±1.3 kJ/mol, respectively.

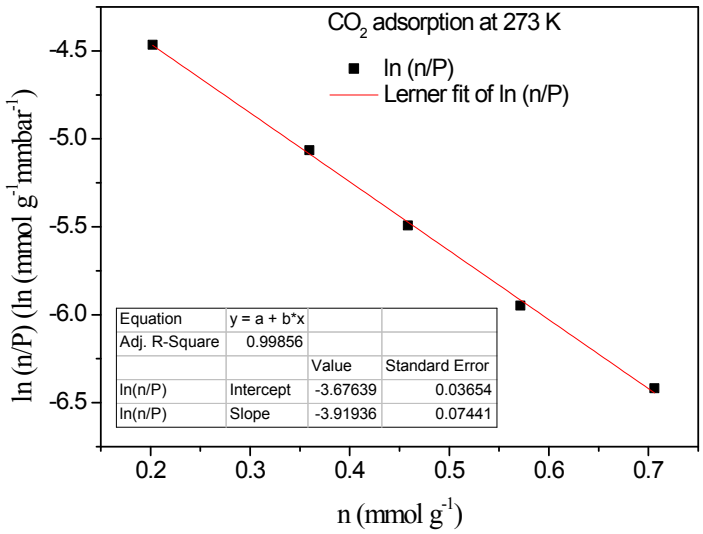

Fig. S10 Virial graph for the adsorption of CO_2 on **1a** at 273 K

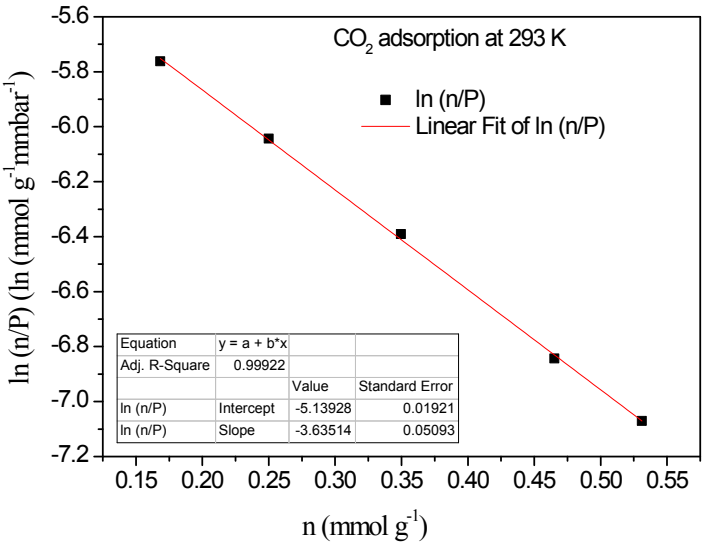

Fig. S11 Virial graph for the adsorption of CO_2 on **1a** at 293 K

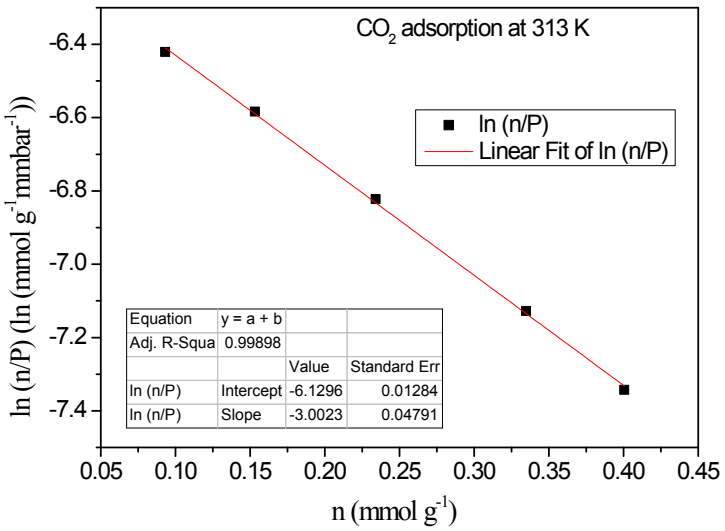

Fig. S11 Virial graph for the adsorption of CO_2 on **1a** at 303 K

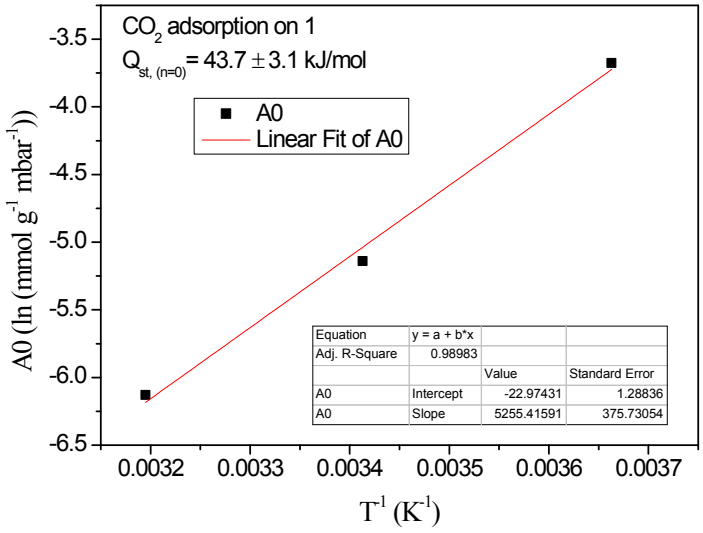

Fig. S12 A graph of A_0 versus 1/T for CO_2 adsorption on **1a**

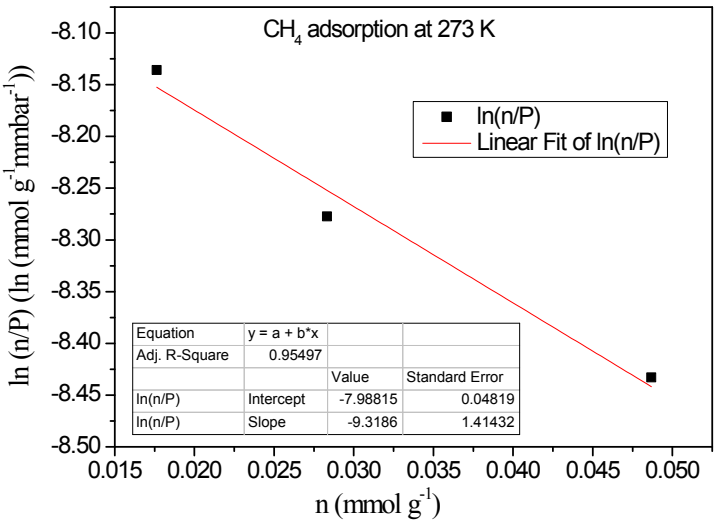

Fig. S13 Virial graph for the adsorption of CH_4 on **1a** at 273 K

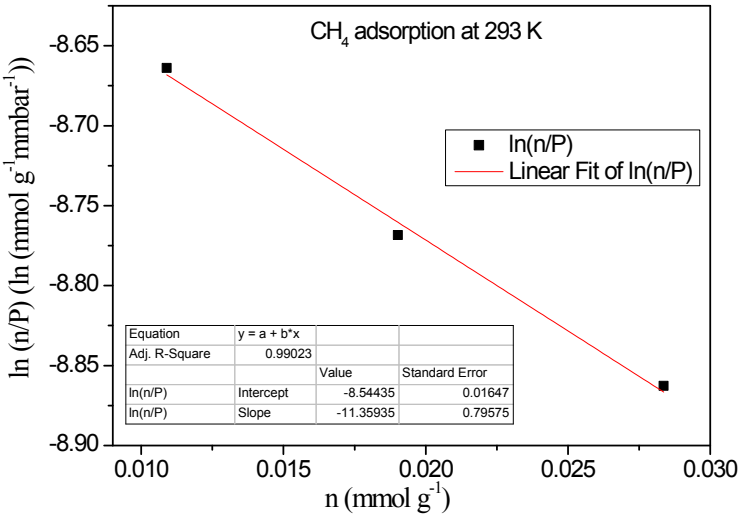

Fig. S14 Virial graph for the adsorption of CH_4 on **1a** at 293 K

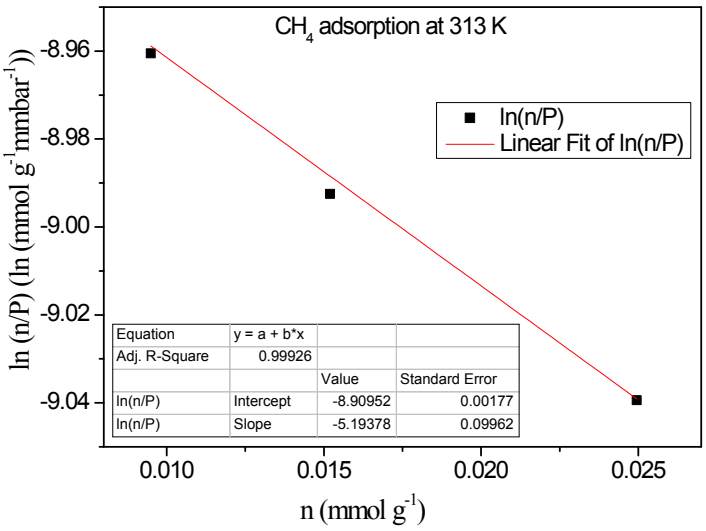

Fig. S15 Virial graph for the adsorption of CH_4 on **1a** at 303 K

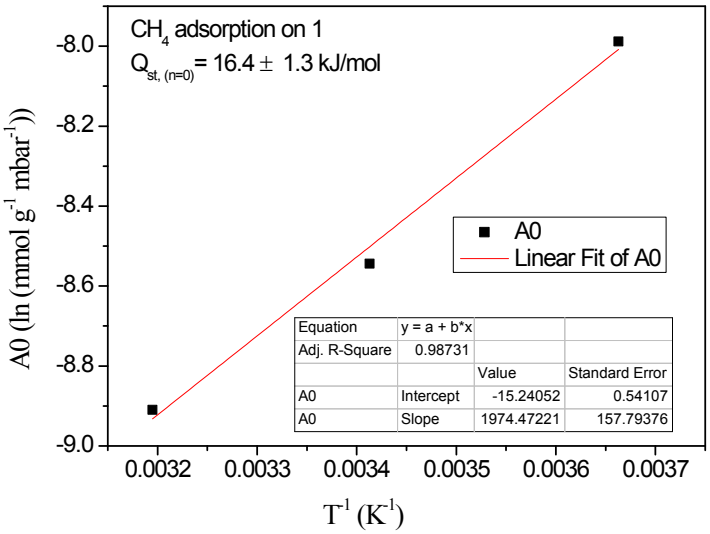

Fig. S16 A graph of A_0 versus 1/T for CH_4 adsorption on **1a**

2. Isosteric heats of adsorption (Q_{st})

Method :

The isosteric adsorption enthalpy of CO_2 and CH_4 were calculated by the Clausius-Clapeyron equation.

$$\frac{Q_{st}}{R} = \frac{d(\ln P)}{d(1/T)} \qquad (13)$$

lnP and 1/T were obtained from the CO_2 and CH_4 isotherms at 273, 293 and 313 K.

As shown in Figs. S17-32, the term lnP exhibits an excellent linear relationship with (1/T), indicating the good reliability of the adsorption data. The slope of lnP versus 1/T was obtained from the linear regression, and Q_{st} was calculated by using the above equation.

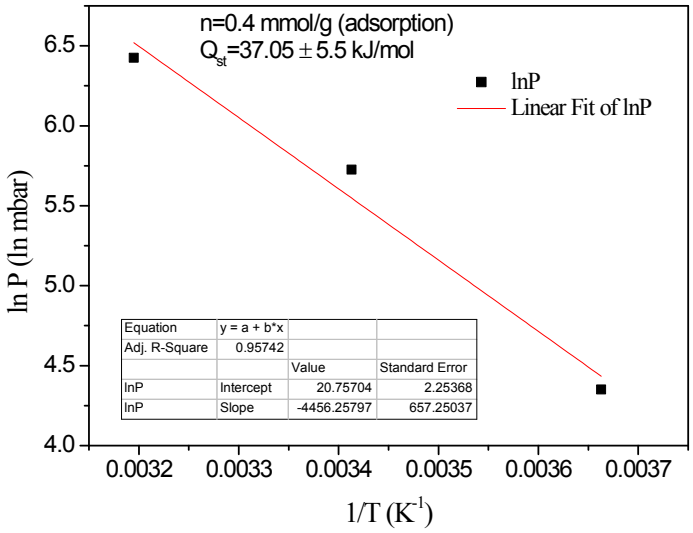

Fig. S17 The Vant' Hoff Isochores for CO_2 adsorption on **1a** (n=0.4 mmol/g)

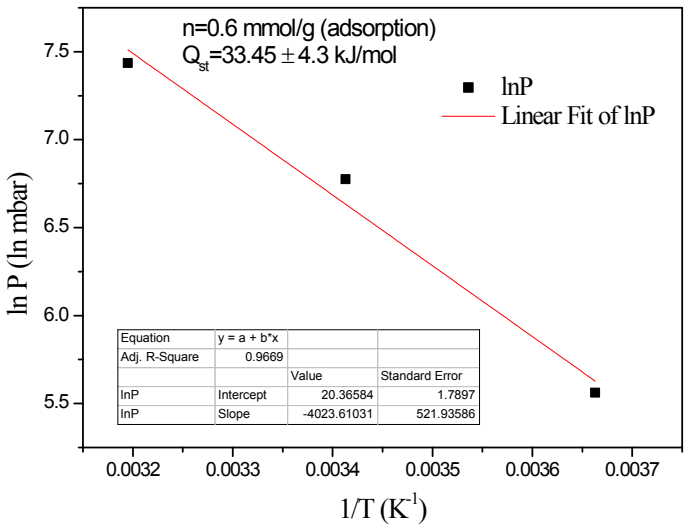

Fig. S18 The Vant' Hoff Isochores for CO_2 adsorption on **1a** (n=0.6 mmol/g)

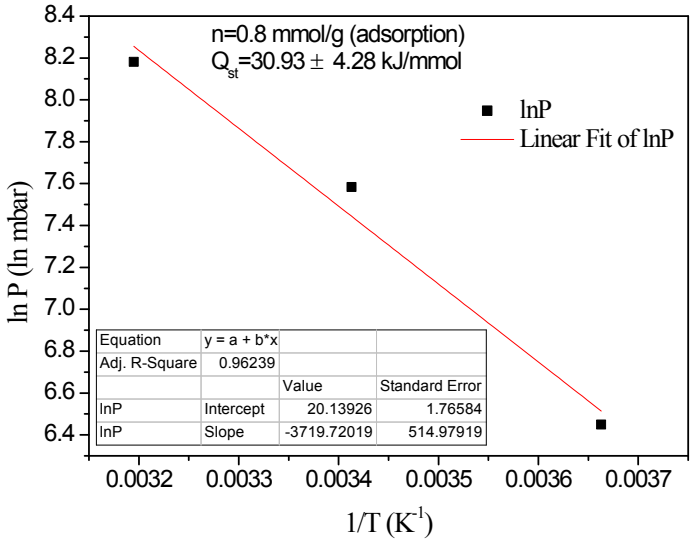

Fig. S19 The Vant' Hoff Isochores for CO_2 adsorption on **1a** (n=0.8 mmol/g)

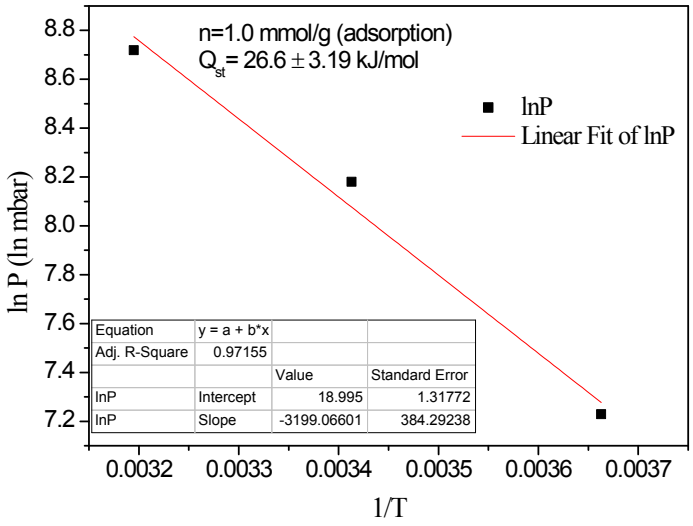

Fig. S20 The Vant' Hoff Isochores for CO_2 adsorption on **1a** (n=1.0 mmol/g)

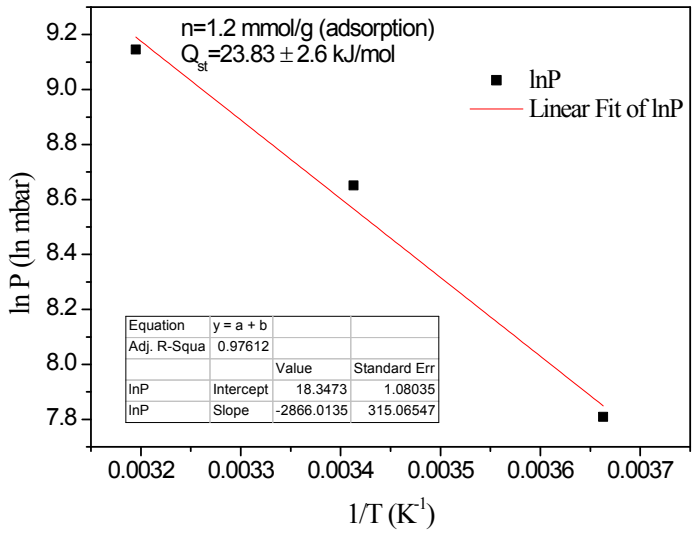

Fig. S21 The Vant' Hoff Isochores for CO_2 adsorption on **1a** (n=1.2 mmol/g)

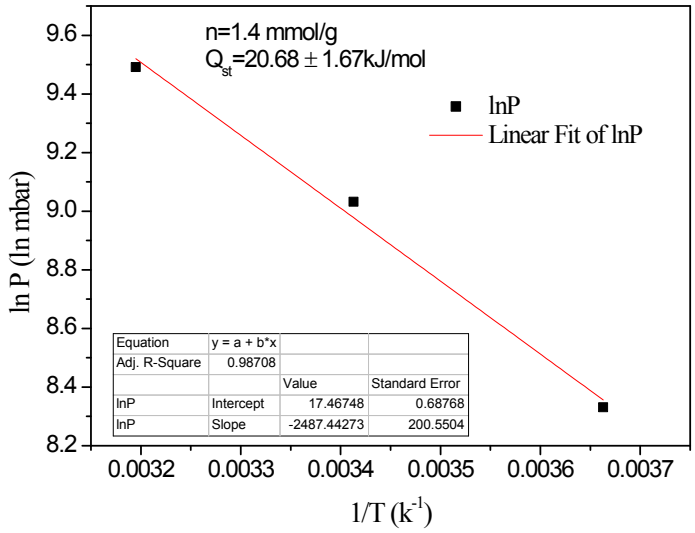

Fig. S22 The Vant' Hoff Isochores for CO_2 adsorption on **1a** (n=1.4 mmol/g)

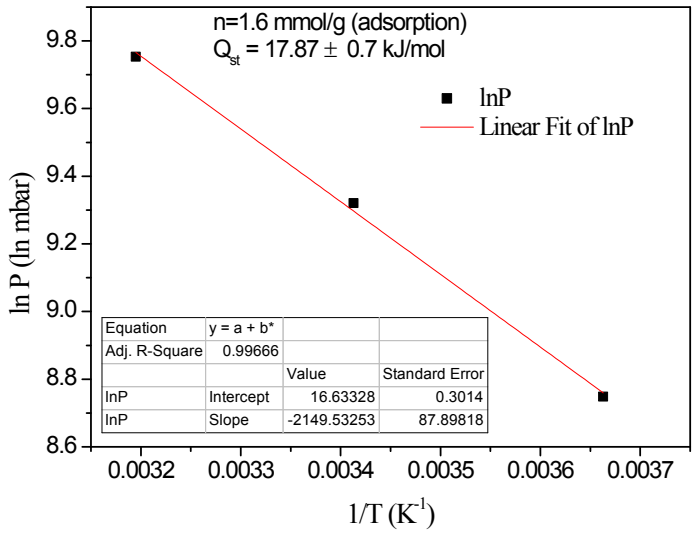

Fig. S23 The Vant' Hoff Isochores for CO_2 adsorption on **1a** (n=1.6 mmol/g)

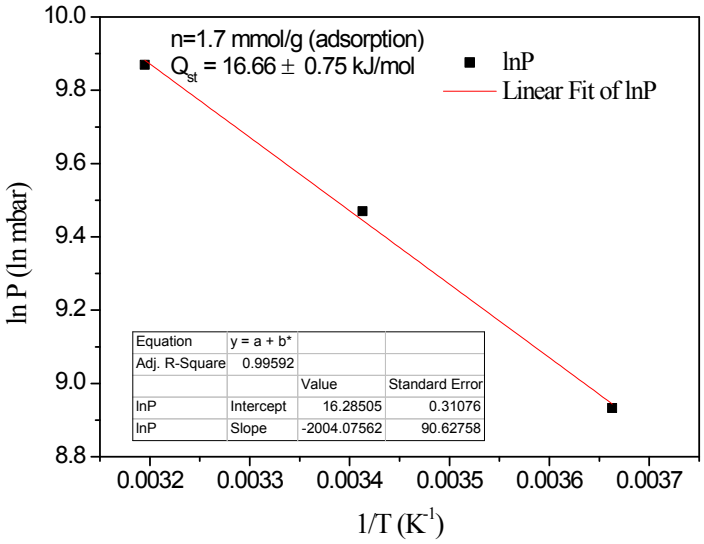

Fig. S24 The Vant' Hoff Isochores for CO_2 adsorption on **1a** (n=1.7 mmol/g)

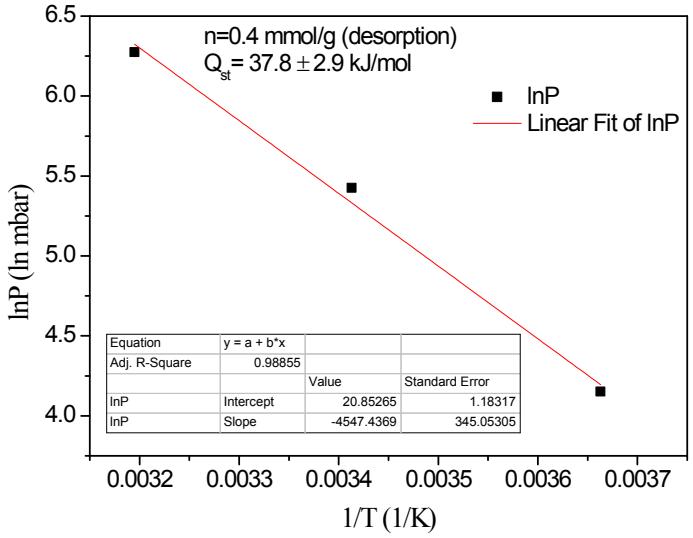

Fig. S25 The Vant' Hoff Isochores for CO_2 desorption on **1a** (n=0.4 mmol/g)

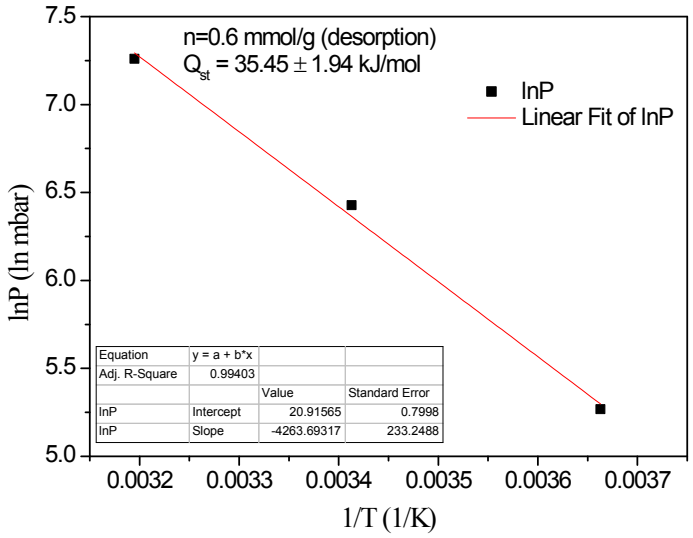

Fig. S26 The Vant' Hoff Isochores for CO_2 desorption on**1a** (n=0.6 mmol/g)

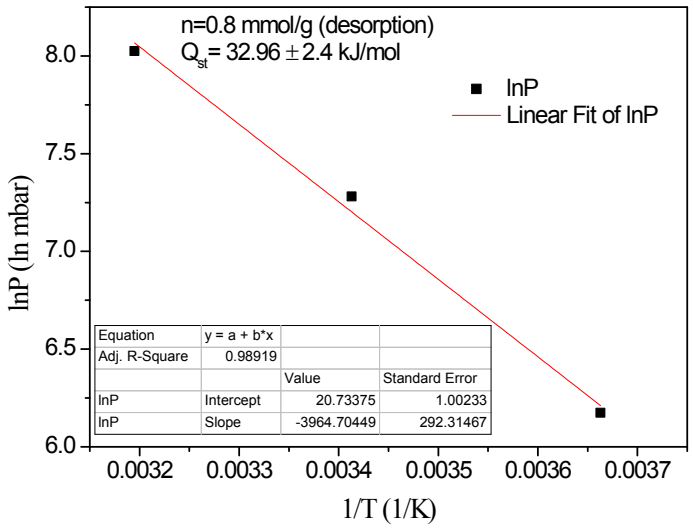

Fig. S27 The Vant' Hoff Isochores for CO_2 desorption on **1a** (n=0.8 mmol/g)

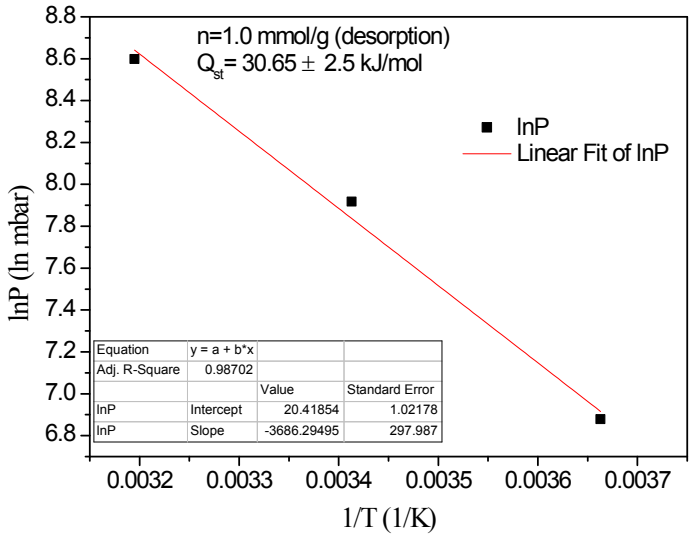

Fig. S28 The Vant' Hoff Isochores for CO_2 desorption on **1a** (n=1.0 mmol/g)

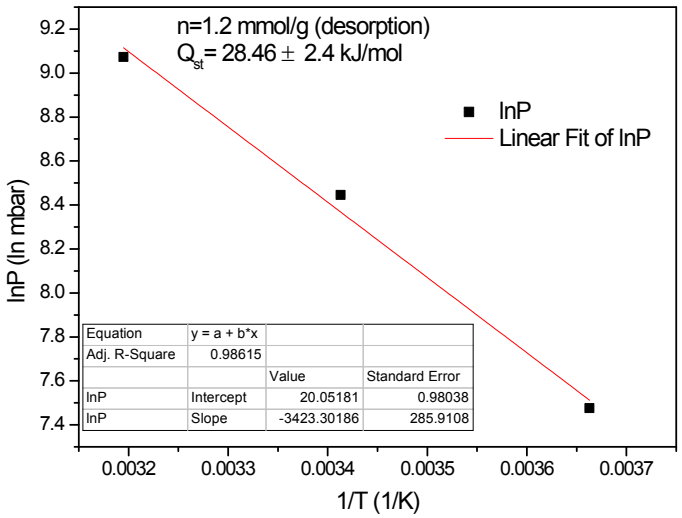

Fig. S29 The Vant' Hoff Isochores for CO_2 desorption on **1a** (n=1.2 mmol/g)

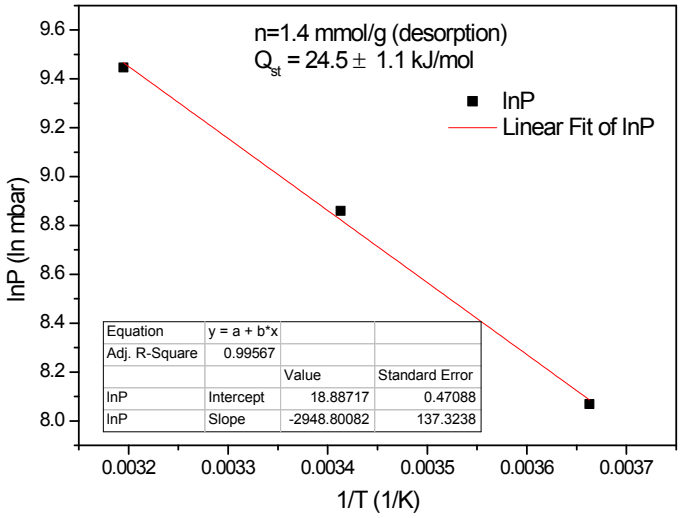

Fig. S30 The Vant' Hoff Isochores for CO_2 desorption on **1a** (n=1.4 mmol/g)

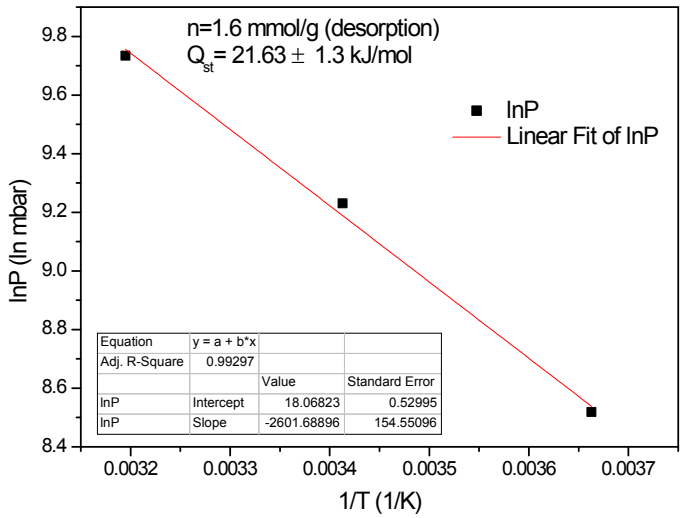

Fig. S31 The Vant' Hoff Isochores for CO_2 desorption on **1a** (n=1.6mmol/g)

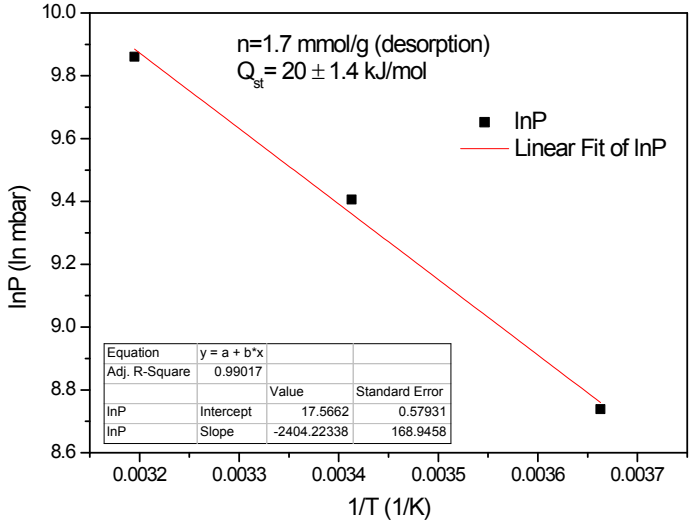

Fig. S32 The Vant' Hoff Isochores for CO_2 desorption on evacuated **1a** (n=1.7mmol/g)

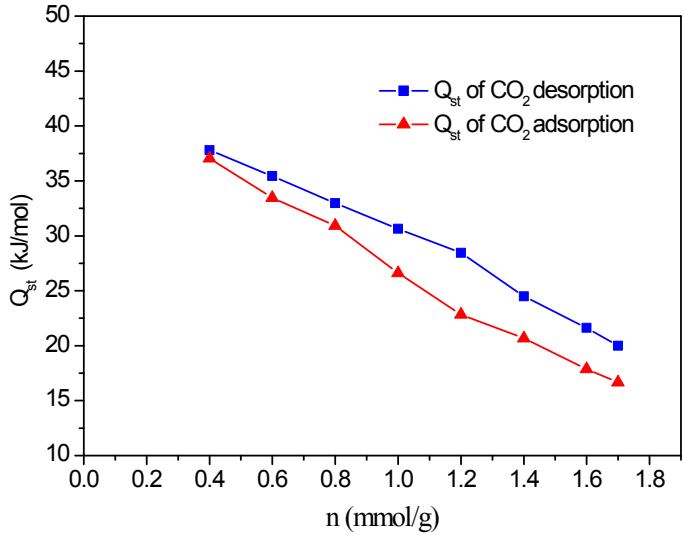

Fig. S33 Isosteric adsorption enthalpies of CO_2 on **1a** from adsorption and desorption branches

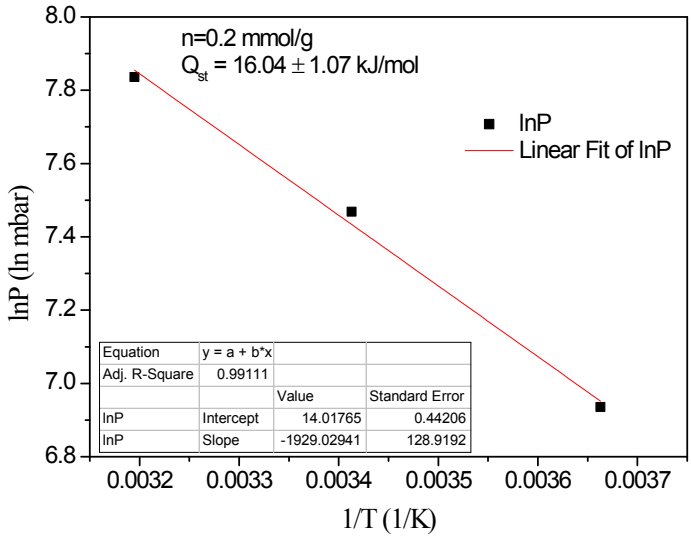

Fig. S34 The Vant' Hoff Isochores for CH_4 adsorption on evacuated **1a** (n=0.2 mmol/g)

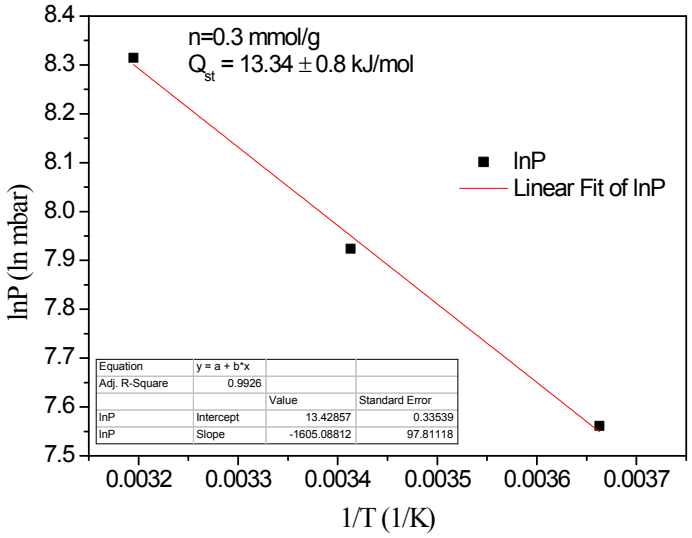

Fig. S35 The Vant' Hoff Isochores for CH_4 adsorption on evacuated **1a** (n=0.3 mmol/g)

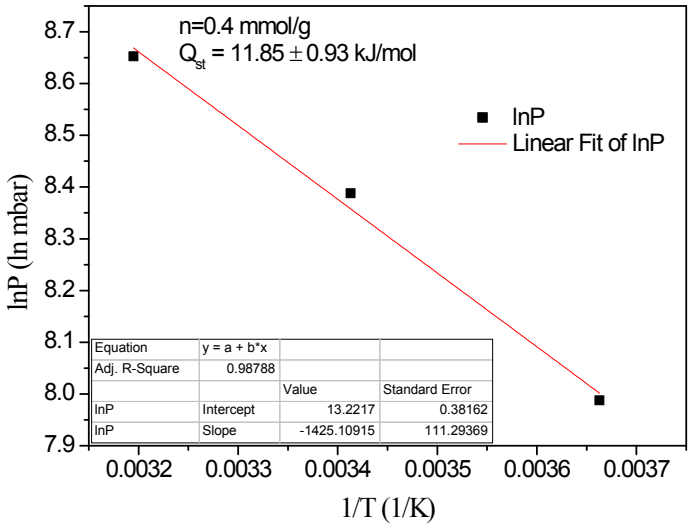

Fig. S36 The Vant' Hoff Isochores for CH_4 adsorption on evacuated **1a** (n=0.4 mmol/g)

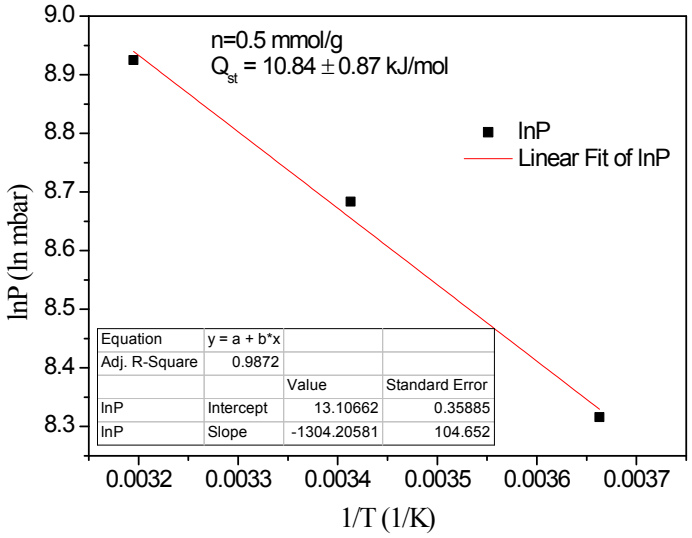

Fig. S37 The Vant' Hoff Isochores for CH_4 adsorption on evacuated **1a** (n=0.5 mmol/g)

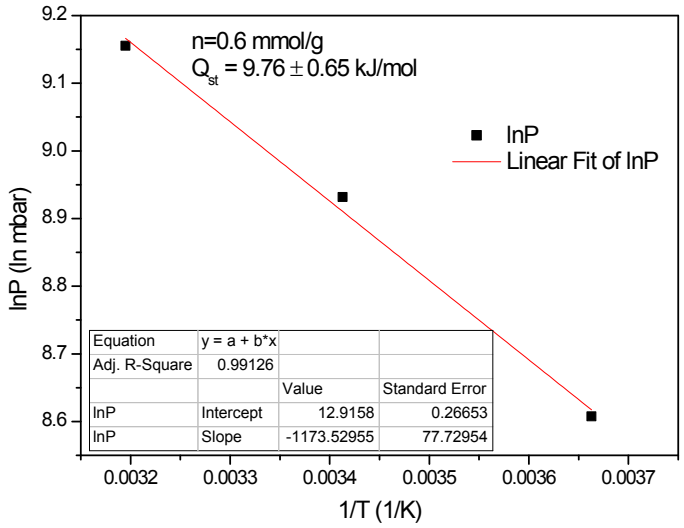

Fig. S38 The Vant' Hoff Isochores for CH_4 adsorption on evacuated **1a** (n=0.6 mmol/g)

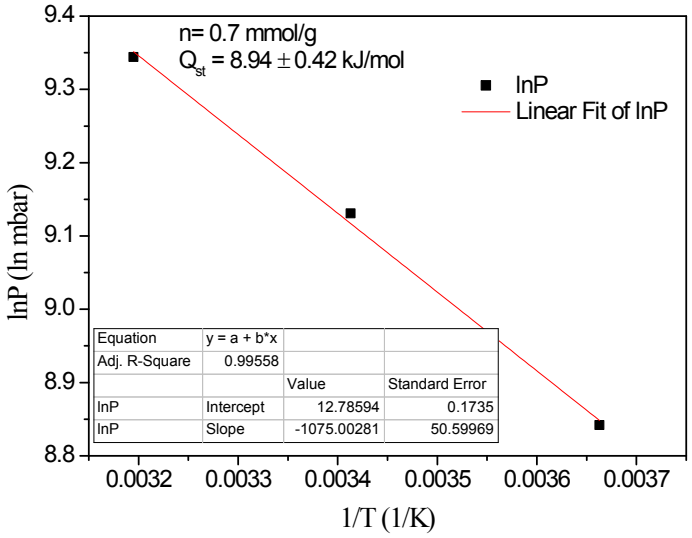

Fig. S39 The Vant' Hoff Isochores for CH_4 adsorption on evacuated **1a** (n=0.7 mmol/g)

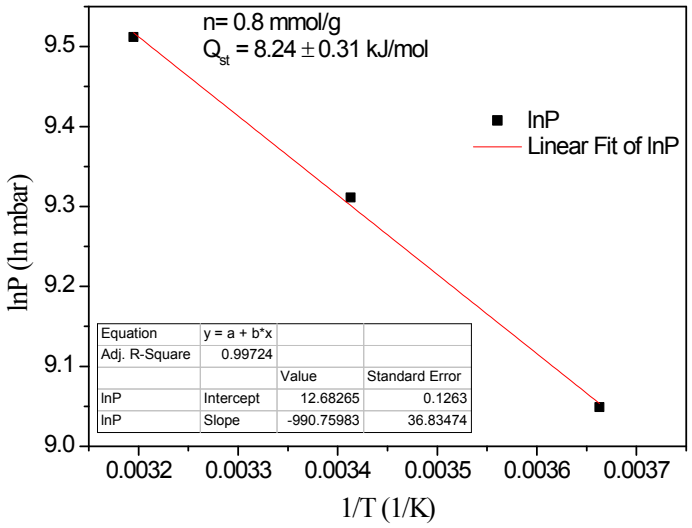

Fig. S40 The Vant' Hoff Isochores for CH_4 adsorption on evacuated **1a** (n=0.8 mmol/g)

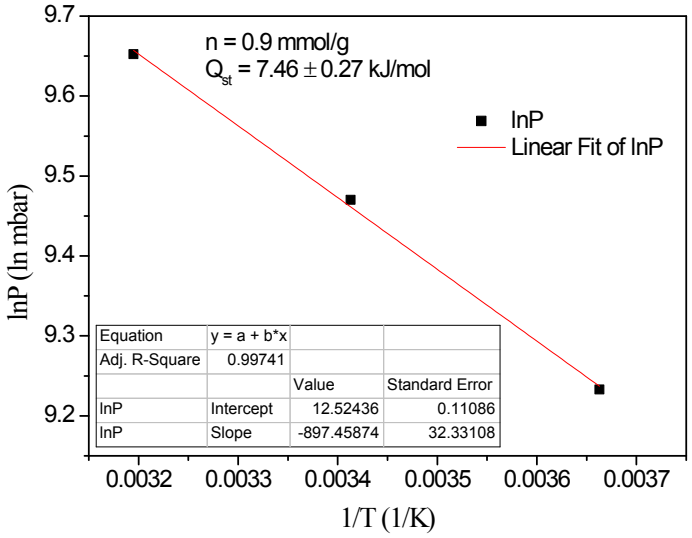

Fig. S41 The Vant' Hoff Isochores for CH_4 adsorption on evacuated **1a** (n=0.9 mmol/g)

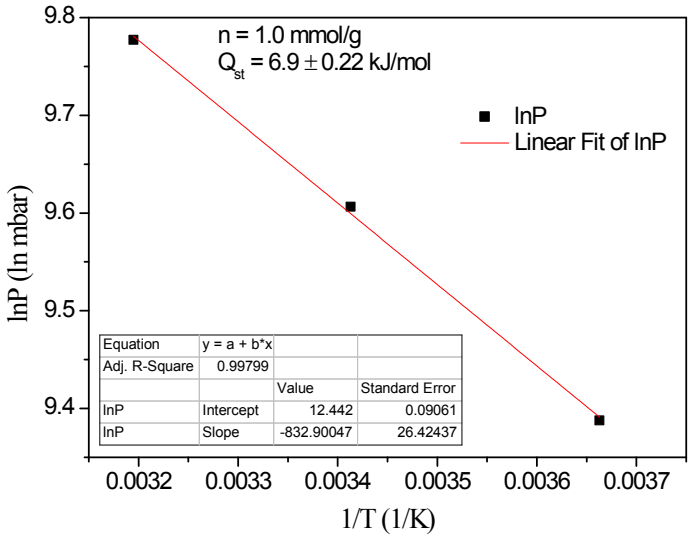

Fig. S42 The Vant' Hoff Isochores for CH_4 adsorption on evacuated **1a** (n=1.0 mmol/g)

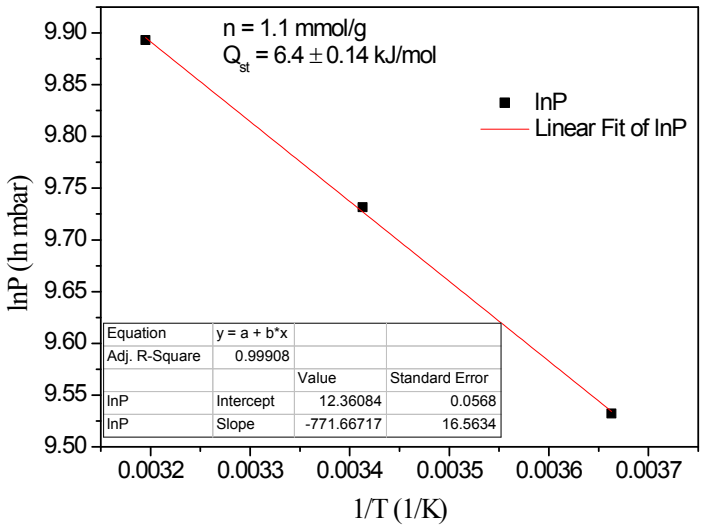

Fig. S43 The Vant' Hoff Isochores for CH_4 adsorption on evacuated **1a** (n=1.1 mmol/g)

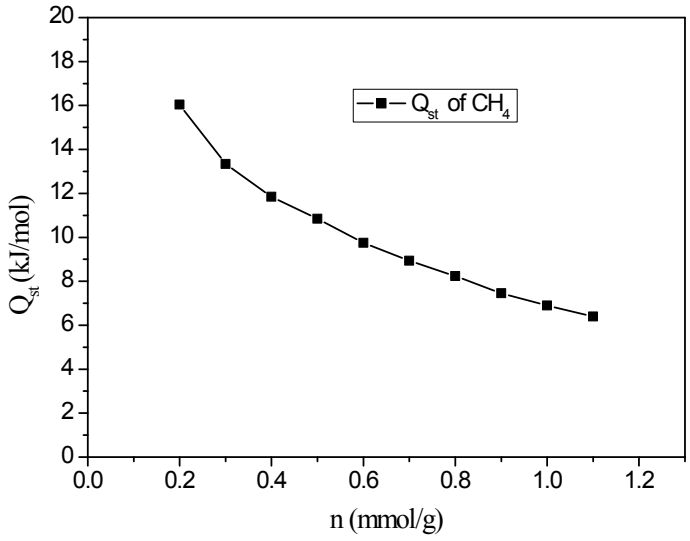

Fig. S44 Isosteric adsorption enthalpies of CH4 on **1a**

Reference

[1] X. Lin, I. Telepeni, A. J. Blake, A. Dailly, C. M. Brown, J. M. Simmons, M. Zoppi, G. S. Walker, K. M. Thomas, T. J. Mays, P. Hubberstey, N. R. Champness, M. Schröder, *J. Am. Chem. Soc.* **2009**, *131*, 2159-2171.

[2] F. S. Mancilha, B. A. DaSilveira Neto, A. S. Lopes, P. F. Moreira, F. H. Quina, R. S. Gonçalves, J. Dupont, *Eur. J. Org. Chem.* **2006**, *2006*, 4924-4933.

[3] G. M. Sheldrick, Madison, WI, , **2003**.

[4] G. M. Sheldrick, University of Gottingen, Gottingen, **1997**.

[5] G. M. Sheldrick, University of Gottingen,, Gottingen, **1997**.

[6] A. L. Spek, Utrecht University, Utrecht, The Netherlands, **2001**.

[7] D. Cazorla-Amorós, J. Alcañiz-Monge, A. Linares-Solano, *Langmuir* **1996**, *12*, 2820-2824.

[8] a) M. Frère, G. De Weireld, R. Jadot, *Journal of Porous Materials* **1998**, *5*, 275-287; b) A. Guillot, F. Stoeckli, *Carbon* **2001**, *39*, 2059-2064.

[9] F. Stoeckli, L. Ballerini, *Fuel* **1991**, *70*, 557-559.

[10] H. Wang, K. Yao, Z. Zhang, J. Jagiello, Q. Gong, Y. Han, J. Li, *Chem. Sci.* **2014**.

[11] A. L. Myers, J. M. Prausnitz, *AIChE J.* **1965**, *11*, 121-127.